Measurement Error in Atomic-Scale STEM-EDS Mapping of a Model Oxide Interface

Steven R. Spurgeon, Yingge Du, and Scott A. Chambers
Physical and Computational Sciences Directorate,
Pacific Northwest National Laboratory, Richland, Washington 99352, USA
(Dated: October 12, 2016)

Atomic-scale characterization tools are increasingly needed to understand the complex composition and chemistry of interfaces, which control the behavior of many desirable emergent properties. While aberration-corrected scanning transmission electron microscopy (STEM) provides one of the most comprehensive local probes of nanostructures, the interpretation of atomically-resolved data is greatly complicated by complex beam-sample interactions. The technique of energy-dispersive X-ray spectroscopy (STEM-EDS) in particular has grown in popularity, since it offers the possibility of elemental mapping over a wide range of ionization energies; however, a clear description of the practical factors that produce errors in atomic-scale maps is needed. Here we describe STEM-EDS measurements of a model perovskite oxide interface, which we interpret in light of multislice simulations to systematically explore the effects of thickness and ionization edge on the apparent composition profile. Our measurements of the same sample in regions of different thickness indicate that interface profiles can vary by as much as 2–5 unit cells, depending on the spectral feature. This finding is supported by simulations, which reveal that on-axis maps of even perfectly abrupt interfaces exhibit significant delocalization. We find that quantification of thicker samples is further complicated by channeling to heavier sites across the interface, as well as an increased signal background. Our study shows that moderately thick samples can suffer from complex channeling effects, resulting in potential misinterpretations of interface structure.

arXiv:1610.03432v1 [cond-mat.mtrl-sci] 11 Oct 2016

Interfaces control the behavior of a variety of emergent properties in oxides, ranging from electron gas formation[1] to ferroelectricity.[2] While great strides have been made in the precision synthesis of atomically-sharp thin film heterostructures,[3] interface charge,[4] strain,[5] and entropy can all drive film-substrate intermixing that can greatly affect properties. The control of interfaces depends on accurate structural characterization; however, commonly used surface analysis techniques, such as X-ray photoelectron spectroscopy (XPS) and secondary ion mass spectroscopy (SIMS) depth profiling, possess coarse lateral spatial resolution and yield area-averaged information on buried interfaces. With the development of commercial spherical aberration (C_S) corrected microscopes, analytical scanning transmission electron microscopy (STEM) is increasingly used to characterize nanoscale interfaces.[6] C_S-correction has enabled the large convergence angles, small probe sizes, and high probe currents needed for efficient chemical mapping of individual atomic columns.[7–10] Complementary analysis using energy-dispersive X-ray spectroscopy (STEM-EDS) and electron energy loss spectroscopy (STEM-EELS) now permits measurements of composition and chemistry at the Ångström scale. While the site-specific nature of these techniques offers rich insight into local interface environments, the interpretation of the resulting data is far from simple and still poorly understood, as discussed in a recent case study of the perovskite $SrTiO_3$ (STO).[11] A complex array of physical factors, including beam broadening and channeling effects,[12] combined with a lack of well-characterized model interfaces, has limited the more widespread adoption of these techniques into the materials science toolkit.

The newly developed technique of atomic-column STEM-EDS mapping exemplifies the challenges associated with the quantification of high-resolution analysis of crystalline materials. In one of the first demonstrations of atomic-scale STEM-EDS mapping of STO,[9] D'Alfonso *et al.* argued that the localization of X-ray scattering potentials can lead to a directly interpretable chemical map analogous to high-angle annular dark field (STEM-HAADF) imaging.[8] However, subsequent work has shown that the contribution of thermally scattered electrons can greatly affect contrast in such chemical maps,[13] while studies of interfaces have revealed that the apparent atomic column size can depend on both channeling and sample thickness.[7,14] Similar difficulties are encountered in STEM-EELS mapping, where image contrast reversals have been observed that are attributed to beam channeling between adjacent atomic columns.[12,15] Probe broadening due to a finite sample thickness can also complicate the analysis of diffuse interfaces. The few quantitative studies conducted to date have shown that the characterization of unknown structures is difficult,[16] generally requiring extensive modeling,[17] and *a priori* sample information.[11]

More study is needed into potential sources of error in STEM-EDS measurements of interface composition and mixing. Here we analyze a model perovskite oxide interface, comparing experimental maps to multislice simulations of an ideal interface. We find that the degree of artificial mixing (measurement error) greatly depends on sample thickness and X-ray ionization edge; moreover, there is strong channeling of the delocalized signal to heavier sites across the interface, which can complicate direct interpretation of peak areas. We find that alloy components can exhibit different thickness dependencies, leading to variations in measurement error for each species. Our study highlights important practical considerations for atomic-scale STEM-EDS mapping of interfaces, emphasizing the need for both extremely thin

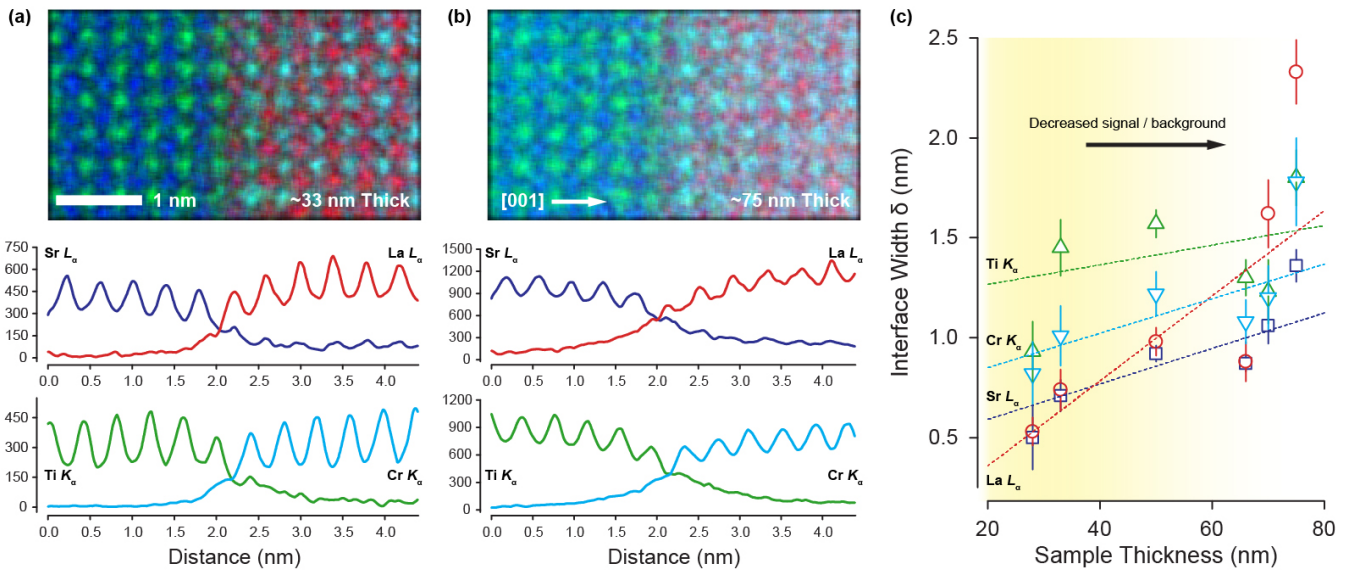

FIG. 1. (a-b) Unfiltered composite STEM-EDS map and corresponding A- and B-site net X-ray count line profiles for ∼33 and ∼75 nm-thick STO / LSCO interfaces, respectively. The line profiles have been averaged in the plane of the maps. (c) Interface width as a function of sample thickness for each edge.

samples and supporting simulations to accurately interpret experimental data.

We have selected a model system consisting of a 30 nm-thick $La_{0.85}Sr_{0.15}CrO_3$ (p-type LSCO) thin film deposited onto a 0.1 Wt% Nb:$SrTiO_3$ (001) (n-type Nb:STO) substrate using molecular beam epitaxy.[18] This system is intriguing for its potential use as an all-perovskite transparent $p-n$ junction, as will be reported elsewhere. Predictive control of device performance depends on a clear understanding of the interface structure to preserve the band offset between the two layers. TEM samples were prepared using a standard lift out method on an FEI Helios DualBeam focused ion beam (FIB) microscope. To generate a range of sample thicknesses, an additional wedge-shaped sample was prepared at 4–7° incidence angle, using ion beam energies of 2–30 keV. STEM measurements were performed at 200 keV using an aberration-corrected JEOL ARM-200CF microscope equipped with a JEOL Centurio silicon drift detector for EDS analysis. All images were acquired along the [100] zone-axis with a ∼ 1 Å probe size and a 27.5 mrad convergence semi-angle, yielding an approximate probe current of ∼ 130 pA. STEM-HAADF images and STEM-EDS maps were acquired at a 90 mrad collection inner semi-angle; the latter was conducted in multiple regions using the Thermo Noran System 7 software, with an approximate instantaneous pixel dwell time of 50 µs px^{-1}, an effective total dwell time of 9–27 ms px^{-1}, and a total collection time of 5–17 min. Maps were processed for net counts, with a background removal and multiple linear least squares fit of reference spectra to deconvolute overlapping peaks. STEM-EELS zero-loss peak thickness measurements indicate that the measured regions are approximately 28, 33, 50, 66, 70, and 75 nm-thick.

Multislice simulations were conducted using the quantum excitation of phonons (QEP) model,[19] which accounts for beam channeling effects and allows for separation of elastic and thermal electrons, in contrast to the frozen phonon model. Our simulations used a supercell consisting of three unit cells of TiO_2-terminated $SrTiO_3$ (STO) interfaced with four unit cells of $La_{0.85}Sr_{0.15}CrO_3$ (LSCO). STEM-EDS ionization maps were simulated using the µSTEM v4.4 software package[20] with a 8×1 supercell tiling and 512×512 px grid sampling for 10, 25, 50, and 100 nm-thick crystals. Crystal models were converted into the appropriate input format using the XTL-Converter program.[21] A Gaussian finite source correction (FWHM = 0.1 nm) was applied to the resulting ionization maps.

Figures 1(a-b) show composite STEM-EDS maps and corresponding averaged line profiles for Sr L_α (1.806 kV), La L_α (4.650 kV), Ti K_α (4.508 kV), and Cr K_α (5.412 kV) taken from ∼33 and ∼75 nm-thick regions, respectively. The profiles were extracted from the net X-ray counts maps, averaged in the film plane, and smoothed using an adjacent averaging filter. For comparison to simulation, we propose the use of a logistic fit to the extrema on either side of the interface; we define the interface width (δ) as the difference of 90% and 10% of the signal maxima. Using this procedure we measure the interface width as a function of sample thickness, as shown in Figure 1(c). Even though all measurements are conducted on the same crystal, we find that there is a clear increase in the apparent interface width in thicker mapping regions. δ_{La} by far exhibits the largest change in interface width, increasing nearly fourfold by ∼ 1.8 nm

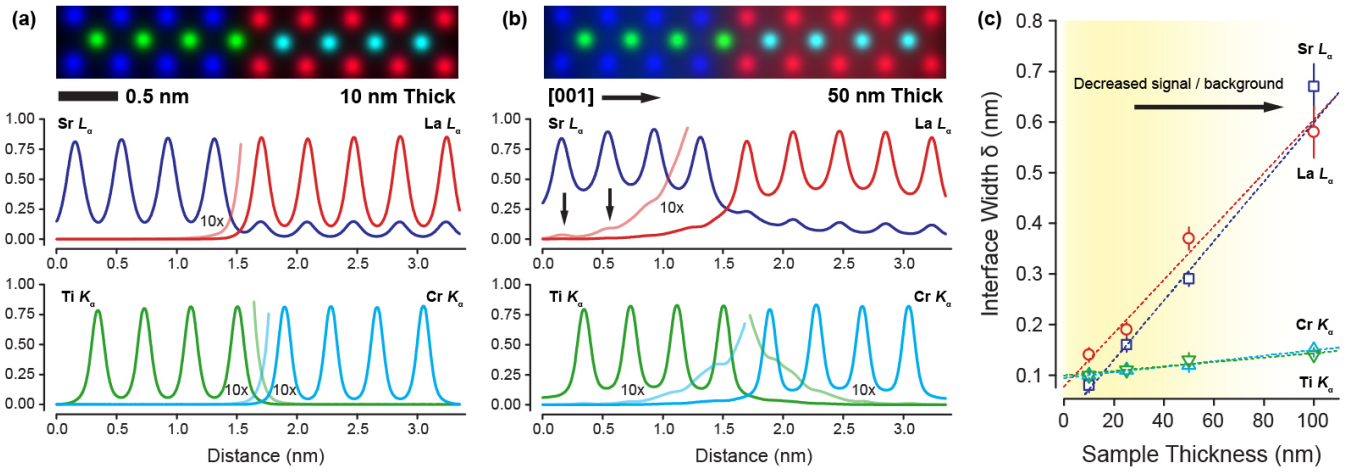

FIG. 2. (a-b) Simulated STEM-EDS ionization maps and corresponding A- and B-site line profiles for abrupt 10 and 50 nm-thick STO / LSCO interfaces, respectively. The line profiles have been normalized to the signal maxima and are inset with a 10× magnified signal to emphasize channeling effects. (c) Interface width as a function of model thickness for each edge.

moving from 28 to 75 nm-thick regions. δ_{Sr} and δ_{Cr} increase by ~ 0.86 and ~ 0.96 nm, respectively, while δ_{Ti} increases by ~ 0.87 nm. Depending on the species, these values correspond to nearly 2–5 unit cells of measurement error. We find that the absolute value of δ_{Ti} is generally larger than the other species in the thinnest regions; significant Ti interdiffusion is not unexpected in this system and may actually promote a more stable interface.[22] In addition to the broadening of interface profiles, we also find that the peak-to-background ratios of the profiles significantly decrease with increasing thickness, as evidenced by comparing Figures 1(a-b). These results are troubling and suggest that the accuracy of interface measurements, as well as the quantification of resulting peak areas, can greatly depend on sample preparation.

To gain insight into the effects of delocalization and channeling on the resulting ionization maps, we have performed multislice simulations, systematically varying the thickness of a model interface. We consider an ideal abrupt STO / $La_{0.85}Sr_{0.15}CrO_3$ interface, thereby avoiding the complications of modeling different interface geometries. We have simulated ionization maps for 10, 25, 50, and 100 nm-thick samples; selected ionization maps and line profiles for the 10 and 50 nm-thick samples are shown in Figures 2(a-b), respectively, alongside a plot of interface width *versus* crystal thickness in Figure 2(c). A comparison of the maps in Figures 2(a-b) shows that the 50 nm-thick sample exhibits a higher background than the 10 nm-thick sample, as indicated by the diffuse bands of contrast between lattice sites. Figure 2(a) shows line profiles taken from both the A- and B-site columns of the 10 nm-thick sample; here we find that the ionization signal of all four edges is strongly localized to their respective atomic columns, with a low background between peaks. This case corresponds to the ultrathin limit previously described by Lu *et al.*,[7] where the electron wave is, in principle, directly convoluted with the local EDS ionization potential and is minimally influenced by beam channeling effects. Using the same logistic fitting procedure we measure the following interface widths: $\delta_{\mathrm{Sr}} = 0.08$, $\delta_{\mathrm{Ti}} = 0.10$, $\delta_{\mathrm{La}} = 0.14$, and $\delta_{\mathrm{Cr}} = 0.10$ nm (all ± 0.01 nm). While our simulations cannot account for all factors, such as thickness or strain fluctuations across the interface, we estimate that this result represents the lower limit of intermixing measurements in an extremely thin and abrupt interface. Even in the case of such an ideal sample, there is still some artificial intermixing; moreover, this intermixing is nearly 50% larger for the A-site ionization as compared to the B-sites, suggesting that the choice of ionization edge is important.

Line profiles from the 50 nm-thick model, shown in Figure 2(b), reveal very different behavior from the 10 nm-thick case. The background between lattice sites has significantly increased, resulting from increased signal delocalization. Interestingly, while the background for the Sr L_α and La L_α edges is nearly 50% of the signal maximum, the background for the Ti K_α and Cr K_α edges is less than 25% of the maximum. The choice of ionization edge may therefore determine the accuracy of composition quantification based on peak area fitting.[14] Furthermore, the A-site line profiles show that a substantial fraction ($10-15\%$) of the signal can be delocalized across even a perfectly abrupt interface. We find that the delocalized signal for La L_α is channeled to A-sites in the adjacent layer, as marked by the arrows in Figure 2(b); a similar, albeit much reduced, effect is seen for the B-sites. This delocalization and subsequent channeling to heavier sites arises from thermally scattered electrons, which are able to excite secondary ionization events.[13] As expected, delocalization results in a sizable increase in the apparent interface width, yielding: $\delta_{\mathrm{Sr}} = 0.29 \pm 0.01$, $\delta_{\mathrm{Ti}} = 0.12 \pm 0.01$, $\delta_{\mathrm{La}} = 0.37 \pm 0.02$, and $\delta_{\mathrm{Cr}} = 0.13 \pm 0.01$ nm. We again find that delocalization is much more pronounced for the Sr L_α and La L_α signals, almost tripling

δ from $0.12 - 0.13$ to $0.29 - 0.37$ nm. This width corresponds to nearly a unit cell of artificial intermixing (measurement error), even in the case of a perfectly abrupt interface structure. On the other hand, the Ti K_α and Cr K_α signals show only a negligible increase in artificial interface width compared to the 10 nm-thick case.

A comparison to our experiments shows that, even though the measured profiles are several times wider than the simulations, there is a consistent trend toward an artificially broadened interface in thicker regions. In agreement with our simulations, we find that the La L_α signal exhibits the largest increase in broadening, but the other species exhibit similar trends. The La signal delocalization may depend more strongly on thickness, leading to greater uncertainty in its true interface profile. Most importantly, we observe that the absolute value of the interface width can vary by as much as 2–5 unit cells, making it difficult to extract a meaningful picture of the interface in thicker mapping regions. Atomic force microscopy (AFM) measurements of the substrate surface indicate that at most one step is present in the TEM sample, supporting our claim that the broadened interfaces result from increased signal delocalization. In summary, our results highlight three difficulties faced in the quantification of interfaces: first, delocalization can give rise to sizable artificial intermixing of several unit cells for common sample thicknesses; second, signal channeling to heavier sites and an increased background greatly complicate quantification based on peak areas; and third, interface measurement error may depend on the choice of ionization edge.

In light of these results, great care must be taken to conduct meaningful analyses of interfaces using the STEM-EDS technique. We find that delocalization effects are minimized in the thinnest regions and that the best results are obtained below 25–30 nm; however, this imposes a severe limit on sample preparation and signal collection times for accurate quantification. We also emphasize that multislice simulations should be conducted for each system and ionization edge of interest to aid the interpretation of experimental data. Future GPU-accelerated computing will allow us to produce more rigorous models to better simulate real-world interfaces and help us account for complex delocalization processes.

S.R.S. thanks Drs. Scott Findlay, Yuanyuan Zhu, Despoina Kepaptsoglou, and Matthew Olszta for insightful discussions. This work was supported by the U.S. Department of Energy (DOE), Office of Science, Division of Materials Sciences and Engineering under award #10122. This work was performed in the Environmental Molecular Sciences Laboratory (EMSL), a national science user facility sponsored by the DOE Office of Biological and Environmental Research (BER) and located at Pacific Northwest National Laboratory (PNNL), operated for DOE by Battelle. Multislice calculations were performed using PNNL Institutional Computing.

[1] J. Chakhalian, J. W. Freeland, A. J. Millis, C. Panagopoulos, and J. M. Rondinelli, Rev. Mod. Phys. **86**, 1189 (2014).
[2] J. Mannhart and D. G. Schlom, Science **327**, 1607 (2010).
[3] L. Martin, Y.-H. Chu, and R. Ramesh, Mater. Sci. Eng. R Reports **68**, 89 (2010).
[4] N. Nakagawa, H. Y. Hwang, and D. A. Muller, Nat. Mater. **5**, 204 (2006).
[5] P. S. Sankara Rama Krishnan, A. N. Morozovska, E. A. Eliseev, Q. M. Ramasse, D. Kepaptsoglou, W.-I. Liang, Y.-H. Chu, P. Munroe, and V. Nagarajan, J. Appl. Phys. **115**, 054103 (2014).
[6] O. L. Krivanek, G. J. Corbin, N. Dellby, B. F. Elston, R. J. Keyse, M. F. Murfitt, C. S. Own, Z. S. Szilagyi, and J. W. Woodruff, Ultramicroscopy **108**, 179 (2008).
[7] P. Lu, J. Xiong, M. Van Benthem, and Q. Jia, Appl. Phys. Lett. **102**, 173111 (2013).
[8] L. J. Allen, A. J. DAlfonso, B. Freitag, and D. O. Klenov, MRS Bull. **37**, 47 (2012).
[9] A. J. D'Alfonso, B. Freitag, D. Klenov, and L. J. Allen, Phys. Rev. B **81**, 100101 (2010).
[10] D. A. Muller, L. F. Kourkoutis, M. Murfitt, J. H. Song, H. Y. Hwang, J. Silcox, N. Dellby, and O. L. Krivanek, Science **319**, 1073 (2008).
[11] G. Kothleitner, M. Neish, N. Lugg, S. Findlay, W. Grogger, F. Hofer, and L. Allen, Phys. Rev. Lett. **112**, 085501 (2014).
[12] M. P. Oxley, M. Varela, T. J. Pennycook, K. van Benthem, S. D. Findlay, A. J. D'Alfonso, L. J. Allen, and S. J. Pennycook, Phys. Rev. B **76**, 064303 (2007).
[13] B. D. Forbes, A. J. D'Alfonso, R. E. A. Williams, R. Srinivasan, H. L. Fraser, D. W. McComb, B. Freitag, D. O. Klenov, and L. J. Allen, Phys. Rev. B **86**, 024108 (2012).
[14] P. Lu, E. Romero, S. Lee, J. L. MacManus-Driscoll, and Q. Jia, Microsc. Microanal. **20**, 1782 (2014).
[15] P. Wang, A. J. D'Alfonso, S. D. Findlay, L. J. Allen, and A. L. Bleloch, Phys. Rev. Lett. **101**, 236102 (2008).
[16] P. G. Kotula, D. O. Klenov, and H. S. von Harrach, Microsc. Microanal. **18**, 691 (2012).
[17] M. J. Neish, M. P. Oxley, J. Guo, B. C. Sales, L. J. Allen, and M. F. Chisholm, Phys. Rev. Lett. **114**, 106101 (2015).
[18] K. H. L. Zhang, Y. Du, A. Papadogianni, O. Bierwagen, S. Sallis, L. F. J. Piper, M. E. Bowden, V. Shutthanandan, P. V. Sushko, and S. A. Chambers, Adv. Mater. **27**, 5191 (2015).
[19] B. D. Forbes, A. V. Martin, S. D. Findlay, A. J. D'Alfonso, and L. J. Allen, Phys. Rev. B **82**, 104103 (2010).
[20] L. Allen, A. DAlfonso, and S. Findlay, Ultramicroscopy **151**, 11 (2015).
[21] S. R. Spurgeon, "XTL-Converter v1.1," `http://www.github.com/stevenspurgeon/xtl-converter` (2015).
[22] R. Colby, L. Qiao, K. H. L. Zhang, V. Shutthanandan, J. Ciston, B. Kabius, and S. A. Chambers, Phys. Rev. B **88**, 155325 (2013).